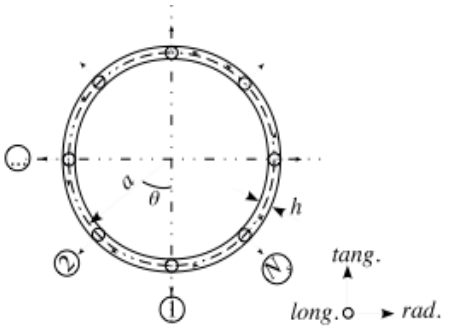

Figure 3. Cross-section of a thin-shell divided into N_s nodes.

Before combining the systems in (6) and (10), two transformations are carried out. First, the soil's FRF matrix is modified to relate displacements to forces instead of tractions by dividing it by the area of the elements in the BE mesh. Second, the tunnel's FRF matrix is modified ($\mathbf{H}^c_t$) to relate displacement and forces in the Cartesian coordinates rather than in the cylindrical coordinates, as

$$\mathbf{H}^c_t = \mathbf{T}'_{r1}\mathbf{H}_t\mathbf{T}_{r1}, \tag{11}$$

where the size of the transformation matrix $\mathbf{T}_{r1}$ is $3N_s \times 3N_s$.

Now, the two systems can be coupled in the wavenumber domain by applying compatibility of displacements and equilibrium of forces at the interface. The equations read,

$$\begin{aligned} \mathbf{U}_s &= \mathbf{H}_s\mathbf{F}_s \\ \mathbf{U}_t &= \mathbf{H}^c_t\left(\mathbf{F}_a - \mathbf{F}_s\right) \\ \mathbf{U}_s &= \mathbf{U}_t \\ \mathbf{F}_s &= \left(\mathbf{H}_s + \mathbf{H}^c_t\right)^{-1}\mathbf{H}^c_t\mathbf{F}_a \end{aligned}, \tag{12}$$

where $\mathbf{F}_a$ is the applied force into the tunnel and $\mathbf{F}_s$ is the resulting force applied into the soil. By knowing $\mathbf{F}_s$, the response at any point in the soil can be calculated.

2.3 The piled-foundation model

The piled-foundation is simulated by an elastic bar for axial loading and an Euler-Bernoulli beam for transverse loading. The pile is represented by its centroid axis, which has N_l equally spaced nodes, see Figure 4. At each of these nodes, there are six DoFs representing displacements and rotations in the three directions. The pile is assumed to be constraint free at its ends and any local deformation of the cross-section is neglected.

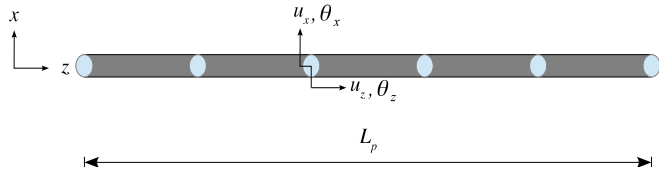

Figure 4. Pile centroid (drawn horizontally) where the circles represent the nodes at which the forces are applied and the responses are calculated. Only the *x*-*z* plane is shown.

The response of the pile to a unit harmonic force with angular frequency ω applied in the longitudinal direction (z) at node j is calculated as follows:

$$\begin{aligned} u_z(z,\omega) &= u^I{}_z = A^I\cos\alpha z + B^I\sin\alpha z \quad \text{for } 0 \le z \le z^j \\ u_z(z,\omega) &= u^{II}{}_z = A^{II}\cos\alpha z + B^{II}\sin\alpha z \quad \text{for } z^j \le z \le L_p \end{aligned}, \tag{13}$$

where $\alpha = \omega\sqrt{\dfrac{\rho_p}{E_p}}$, the superscripts I and II indicate the sections above and beneath the node j and coefficients A^I, B^I, A^{II}, B^{II} are found from the boundary conditions.

The general response of the pile to a unit harmonic force or moment with angular frequency applied in/around the transverse directions (x, y) at node j reads

$$\begin{aligned} u_{x,y}(z,\omega) &= u^I{}_{x,y} = A^I e^{\beta z} + B^I e^{i\beta z} + C^I e^{-\beta z} + D^I e^{-i\beta z} \quad \text{for } 0 \le z \le z^j \\ u_{x,y}(z,\omega) &= u^{II}{}_{x,y} = A^{II} e^{\beta z} + B^{II} e^{i\beta z} + C^{II} e^{-\beta z} + D^{II} e^{-i\beta z} \quad \text{for } z^j \le z \le L_p \end{aligned}, \tag{14}$$

where $\beta = \left(\dfrac{\rho_p A_p \omega^2}{E_P I_p}\right)^{\frac{1}{4}}$ and the coefficients A^I, B^I, C^I, D^I, A^{II}, B^{II}, C^{II}, D^{II} are found from the boundary conditions. In order to obtain the rotation around the transverse direction equation (14) is differentiated with respect to z.

The general solution of the pile to a unit harmonic torque with angular frequency ω applied around the longitudinal direction (z) is,

$$\begin{aligned} \theta_z(z,\omega) &= \theta^I{}_z = A^I\cos\lambda z + B^I\sin\lambda z \quad \text{for } 0 \le z \le z^j \\ \theta_z(z,\omega) &= \theta^{II}{}_z = A^{II}\cos\lambda z + B^{II}\sin\lambda z \quad \text{for } z^j \le z \le L_p \end{aligned}, \tag{15}$$

in which $\lambda = \omega\sqrt{\dfrac{\rho_p}{G_p}}$ and coefficients A^I, B^I, A^{II}, B^{II} are found from the boundary conditions.

Likewise the tunnel, the FRF matrix of the pile's centroid ($\mathbf{H}_l$) can be assembled which has a size of $6N_l \times 6N_l$. This matrix is then transformed to give the FRF matrix ($\mathbf{H}_p$) of the pile's nodes around the circumference as,

$$\mathbf{H}_p = \mathbf{T}'_{r2}\mathbf{H}_l\mathbf{T}_{r2}, \tag{16}$$

where the matrix $\mathbf{H}_p$ has a size of $3N_s \times 3N_s$ and the size of the transformation matrix $\mathbf{T}_{r2}$ is $6N_l \times 3N_s$.

To this end, the systems in (6) and (16) can be coupled in the same way as in (12).

3 MODEL PARAMETERS AND COMPARISONS

In this paper, only the results of the uncoupled system, i.e. sub-models 1 and 2 in Figure 2, are presented. The model of the tunnel is validated against the PiP model [9], which carries out the computations assuming that the tunnel's near field displacement is not influenced by the free surface. The PiP simulates the vibration of a tunnel embedded in a half-space in three steps. First, the model calculates the displacement at the tunnel-soil interface using a model of a tunnel embedded in a full-space. It then calculates equivalent internal forces in a model of a full-space, without a tunnel, that produce the same displacements at the tunnel-soil interface as computed in the first step. Finally, the PiP considers a half-space model, without a tunnel, and multiplies its Green's functions by the equivalent forces in the second step.

For comparisons, a scenario of a tunnel embedded at a depth of 5m and subject to a harmonic point load at its invert is considered. The responses are calculated in the frequency

range 1-80Hz. The number of elements in the BE mesh, which is 40 constant node-collocated elements of equal size, conforms to the number of elements in the tunnel. The parameters used in modelling are summarised in Table 1.

Table 1. Tunnel and soil parameters used for calculating the results of current model and PiP model.

Parameter	Symbol	Value
Tunnel		
Radius	a	2.75m
Density	ρ	2500kg/m^3
Young's modulus	E	50GPa
Poisson's ratio	υ	0.3
Damping loss factor	η	0.03
Soil		
Radius	r	3m
Density	ρ	1800kg/m^3
Shear wave speed	C_s	200m/s
Pressure wave speed	C_p	400m/s
Damping loss factor	η	0.04

The model of the piled-foundation (sub-model 2) is contrasted to the model of Talbot and Hunt [6], which utilised the BE method for the soil applying the fundamental solution of full-space Green's functions. This has led to the discretization of the free surface in order to account for the half-space behaviour. Another feature of Talbot and Hunt's model is that it represented the circular cross-section of the pile by four elements in order to ease the discretization of the free surface using rectangular elements. The current model has 16 constant node-collocated elements in its circumference and 16 constant node-collocated elements in the longitudinal direction. The number of elements in the BE mesh is equal to that in the pile's model.

The responses of the pile due to axial and transverse loading are considered in this paper. These are presented in the form of *flexibility coefficients* $F_{ij} = I_{ij} + iJ_{ij}$, which are obtained by normalising the driving-point FRFs to their static values. Table 2 gives the parameters used in modelling the piled-foundation.

Table 2. Piled-foundation and soil parameters used for calculating the results of the current model and Talbot and Hunt's model.

Parameter	Symbol	Value
Piled-foundation		
Length	L_p	7.5m
Radius	r_p	0.35m
Density	ρ_p	1687kg/m^3
Young's modulus	E_p	25GPa
Poisson's ratio	υ	0.25
Soil		
Radius	r	0.35m
Density	ρ	2250kg/m^3
Shear wave speed	C_s	200m/s
Pressure wave speed	C_p	490m/s
Damping loss factor	η	0.03

4 RESULTS AND DISCUSSION

In this section, the results of the current model are presented and compared against previous models in the literature.

4.1 The tunnel model results

The first set of the results considers the vertical displacements on the free surface (z = 0) at the points (20m, 0m, 0m) and (20m, 20m, 0). Such results are particularly important for practicing engineers to assess underground railway and design mitigation.

Figure 5 depicts the modulus of the vertical displacement (U_z) at the point (20m, 0m, 0m), calculated with the current model and the PiP model. Some differences between both solutions can be seen in the frequency range of 1-20Hz and also in the range of 60-80Hz. However, at mid-range frequencies (25-55Hz) the models compare reasonably well.

The vertical displacement (U_z) modulus computed by the two models at the point (20m, 20m, 0m) on the free surface is presented in Figure 6. The models show at some frequencies reasonable agreement. However, differences of about 10dB are observed around the frequency range 20-30Hz.

The reason of these discrepancies in Figure 5 and Figure 6 could be attributed to a number of reasons. One is that the PiP model simulates the tunnel using continuum theory, which is more robust than the thin-shell theory adopted in the current model. Another reason that could cause such differences is the reflections of waves from the free surface. The PiP model does not include a free surface. A third could be due to the discretization rules followed in developing the BE model and also in the wavenumber sampling.

Despite the differences between both models in Figure 5 and Figure 6, the predictions of the current model are promising and could be further improved following more investigations. It is essential to ensure that the current model of the tunnel provides adequate predictions for the vibration levels before proceeding to the next steps of coupling the tunnel to the piled-foundation. The tunnel wall could also be modelled as a continuum (i.e. thick-wall theory) instead of using the thin-shell theory. However, this is unlikely to make a difference over the frequency range under consideration.

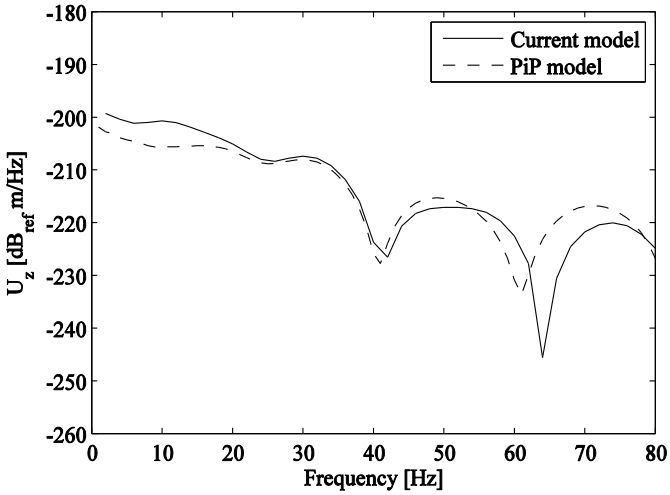

Figure 5. Modulus of the vertical displacement at the point (20m, 0m, 0m) on the free surface computed by the current model and the PiP model.

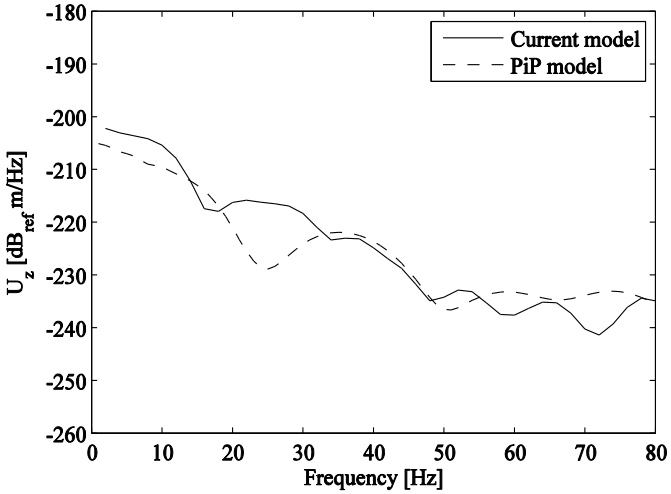

Figure 6. Modulus of the vertical displacement at the point (20m, 20m, 0m) on the free surface computed by the current model and the PiP model.

The second set of results deals with displacement fields on the free surface at frequencies 10Hz and 50Hz. These are only presented for the current model. Waves generated at the tunnel due to the harmonic load at its invert propagate through the soil and result in Rayleigh waves at the surface of the half-space.

In Figure 7, the horizontal displacement field is illustrated for both frequencies. It can be observed that the displacements through the zero x-axis equal zero due to symmetry. The displacements at other symmetry points are equal in magnitude and opposite in direction.

Figure 8 shows the longitudinal displacement field for both frequencies. All displacements through the plane of zero y-axis equal zero due to symmetry. Along the horizontal axis, the displacements are equal in magnitude and in the same direction, whereas along the longitudinal axis the displacements are equal in magnitude and opposite in direction.

The vertical displacement field is shown in Figure 9. It can be seen that the wavefronts on the surface of the half-space are not cylindrical due to the nature of the source and the dynamic interaction between the soil and the tunnel. In this figure the displacements at the symmetry points are equal in magnitude and opposite in direction.

Based on the parameters provided in Table 1, the Rayleigh wave speed is about 190m/s. This results in a Rayleigh wavelength for the frequency 10Hz of about 19m and for the frequency 50Hz of approximately 3.8m. Indeed, these values are calculated based on the single source of a point harmonic load, which is not the scenario for the results presented in Figure 7 - Figure 9.

It can also be discerned from Figure 7 - Figure 9 that the magnitude of the longitudinal displacement (Figure 8) is less than that of the transverse displacements.

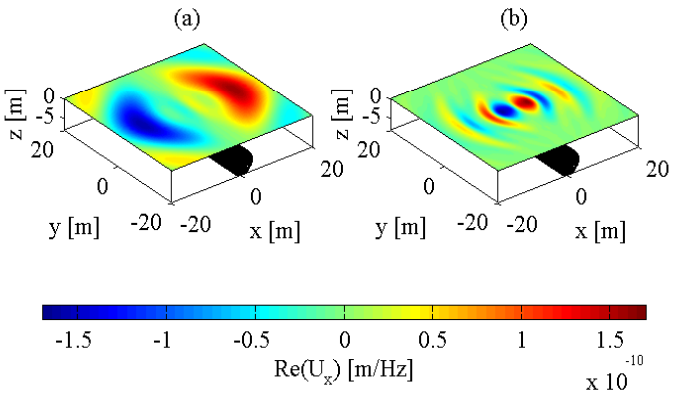

Figure 7. Real part of the horizontal displacement on the free surface at (a) 10Hz and (b) 50Hz computed by the coupled thin-shell-BE model.

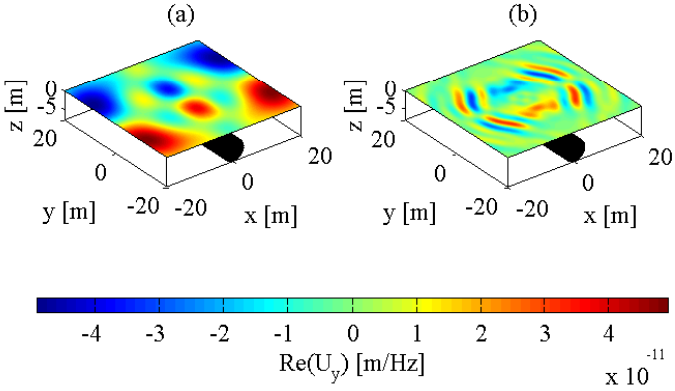

Figure 8. Real part of the longitudinal displacement on the free surface at (a) 10Hz and (b) 50Hz computed by the coupled thin-shell-BE model.

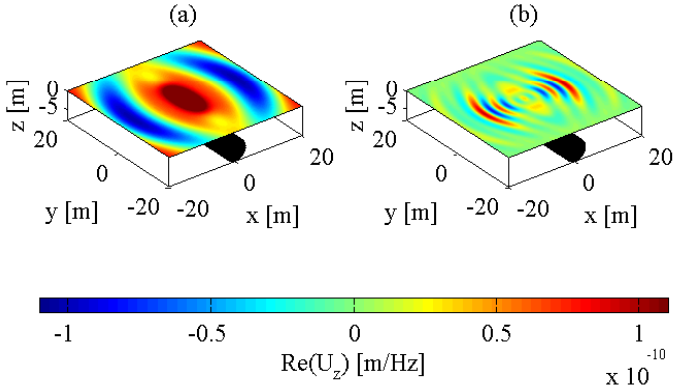

Figure 9. Real part of the vertical displacement on the free surface at (a) 10Hz and (b) 50Hz computed by the coupled thin-shell-BE model.

4.2 The piled-foundation model results

The first part of these results is concerned with presenting the *flexibility coefficients* at the pile-head against non-dimensional frequencies ($a_0=\omega r/C_s$) range from 0 to 0.5. This is the range that was considered in previous work on modelling soil-pile interaction for seismic purposes, in which higher frequencies are not considered.

Figure 10 compares the horizontal pile-head flexibility computed by the current model with those predicted by Talbot and Hunt [6]. The models agree well for both real and imaginary parts at low non-dimensional frequencies. However, small discrepancies are observed at higher frequencies, that are believed to be due to the differences in the size of the BE mesh between the two models. Talbot and Hunt's model used four elements in the circumference whereas the current model utilises 16 elements.

Figure 11 illustrates the vertical pile-head flexibility due to a unit harmonic axial load computed by both models. For the real part flexibility, the difference between the two models is almost constant at all non-dimensional frequencies. For the imaginary part flexibility, however, discrepancies between the models become clearer at frequencies beyond a_0=0.25.

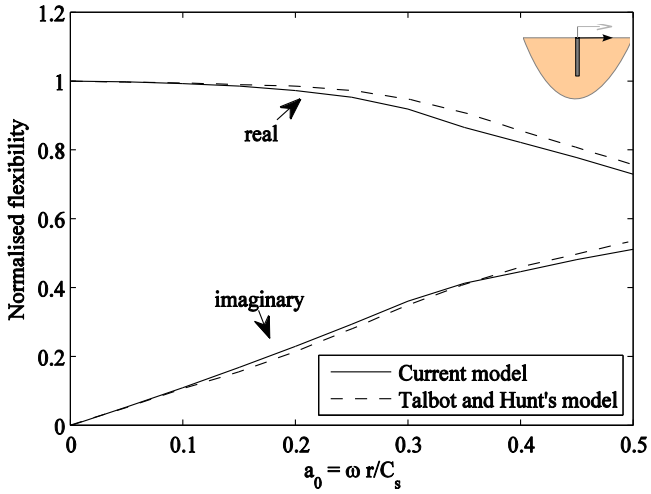

Figure 10. Comparison of the horizontal pile-head *flexibility coefficients* predicted by the current model with those predicted by Talbot's model.

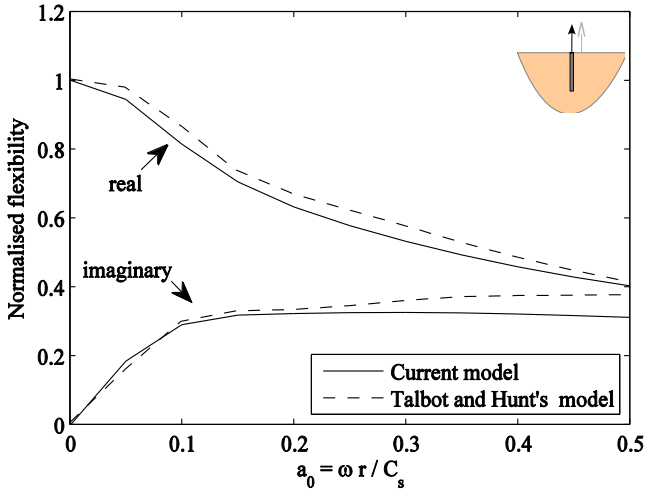

Figure 11. Comparison of the vertical pile-head *flexibility coefficients* predicted by the current model with those predicted by Talbot's model.

Given the differences between the current model and Talbot and Hunt's model in Figure 10 and Figure 11, it can be generally said that the two models are in a good agreement. In essence, the BE mesh of the current model is more adequate as it conforms to the requirements of the mesh size recommended by Dominguez [16]. The current model is also able to predict the dynamic behaviour of the piled-foundation when the pile is subject to torsion – a type of loading that is likely to occur in a fully coupled tunnel-piled-foundation system.

The second part of the piled-foundation results presents the displacement field at the free surface when a unit harmonic vertical point load is applied to the pile-head at a non-dimensional frequency a_0=0.5. Figure 12(a) shows the vertical displacement field at the free surface, where concentric circular wavefronts are observed. This confirms the correctness of the model, as it is expected to have such wavefronts when the piled-foundation is subject to a vertical load on its head.

Figure 12(b) shows a vertical section through the free surface of the displacement field at the location of the pile centroid. The figure indicates the Rayleigh wavelength to be approximately 4.2m. This agrees well with the theoretical Rayleigh wavelength for the parameters in Table 2, which is 4.22m at a_0=0.5. These findings confirm again the accuracy of the current model in predicting the dynamic soil-pile interaction.

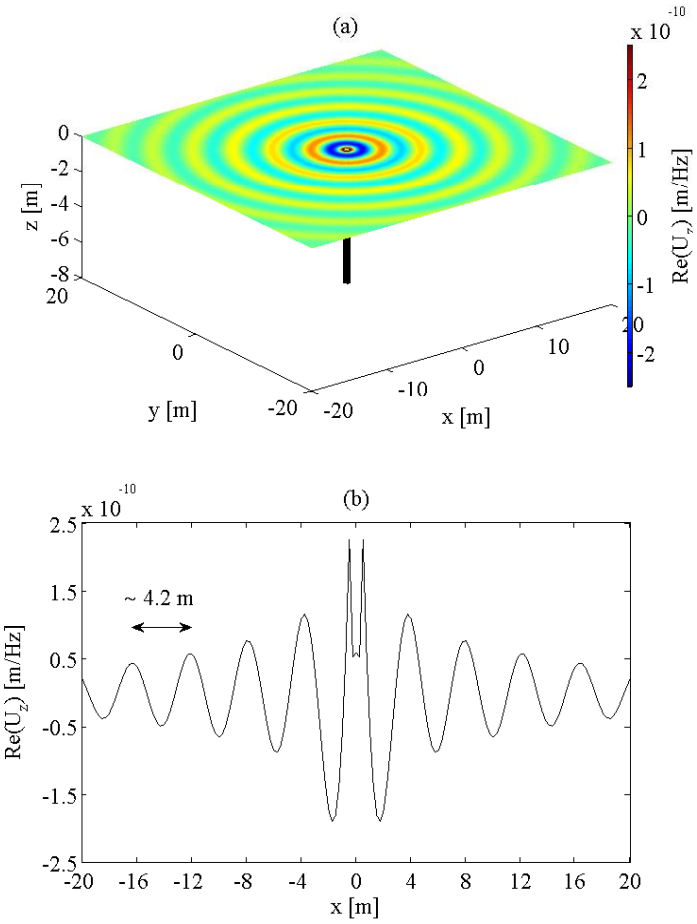

Figure 12. (a) The vertical displacement field predicted by the current model when subject to a point harmonic load on the pile-head at a non-dimensional frequency a_0 = 0.5, (b) vertical section through the free surface at the location of the pile centroid.

5 CONCLUSION AND FUTURE WORK

This paper has proposed a novel technique for modelling the dynamic interaction between an underground tunnel and piled-foundation. The method is based on superposition of vibration wavefields generated by the tunnel and piled-foundation. The soil in this work is modelled using the BE method where half-space Green's functions are used as fundamental solutions. The tunnel is modelled using thin-shell theory, whereas the piled-foundation is modelled using an elastic bar for axial deformation and an Euler-Bernoulli beam for bending deformation.

The paper has first presented the results of the dynamic interaction between a tunnel and soil and compared them against the predictions of the PiP model. The comparisons have revealed that the results of both models agree well at most frequencies. However, some differences between the two models are observed at a number of frequencies. These differences are attributed to the reflection of free surface waves that are not adequately predicted by the PiP model, and also to the discretization rules followed in the BE model.

The paper has also presented the results of the dynamic interaction between the piled-foundation and soil. The model predictions are compared against the BE model of Talbot and Hunt [6] by means of the *flexibility coefficients*. The comparisons include the response of the piled-foundation to a horizontal and vertical point load on the pile-head. It is revealed that both models agree well for the horizontal loading scenario, especially at low frequencies. For the vertical loading scenario, small differences are observed, in particular at higher frequencies.

In general, the presented results have highlighted the ability of the sub-models in adequately predicting the dynamic interaction between the tunnel-soil and soil-piled-foundation. Therefore, the work can now be moved to the next step where both sub-models can be coupled together. The results will then be contrasted to the work of Hussein *et al.* [14], which employed the sub-modelling technique to investigate the dynamic interaction between a railway tunnel and piled-foundation on the basis of weak coupling.

ACKNOWLEDGMENTS

The authors would like to acknowledge the generous funding of the EPSRC (grant reference no. EP/K006665/1) provided to conduct this research. The results presented here are part of the MOTIV (Modelling Of Train Induced Vibration) project. The authors would like also to thank the contribution of the University of KU Leuven for providing the EDT and also for some functions of BEMFUN used in the BE models.

REFERENCES

[1] S. Fidell, D. Barber and T. Schultz, *Updating a dosage-effect relationship for the prevalence of annoyance due to general transportation noise*, J. Acoust. Soc. Am, 89(1), 221-233, 1991.

[2] M. Ferrara and L. De Gennaro, *How much sleep do we need?*, Sleep Med. Rev., 5(2), 155-179, 2001.

[3] X. Sheng, C. Jones and D. Thompson, *Prediction of ground vibration from trains using the wavenumber finite and boundary element methods*, J. Sound Vib., 293, 575-586, 2006.

[4] D. Clouteau, M. Arnst, T. Al-Hussaini and G. Degrande, *Freefield vibrations due to dynamic loading on a tunnel embedded in a stratified medium*, J. Sound Vib., 283, 173-199, 2005.

[5] G. Degrande, D. Clouteau, R. Othman, M. Arnst, H. Chebli, R. Klein, P. Chatterjee and B. Janssesns, *A numerical model for ground-borne vibrations from underground railway traffic based on a periodic finite element-boundary element formulation*, J. Sound Vib., 293, 645-666, 2006.

[6] J. Talbot and H. Hunt, *A computationally efficient piled-foundation model for studying the effects of ground-borne vibration on buildings*, Proc. Inst. IMechE Part C: J. Mech. Eng. Sci., 217, 975-989, 2003.

[7] J. Forrest and H. Hunt, *A three-dimensional model for calculation of train-induced ground vibration*, J. Sound Vib., 294(4-5), 678-705, 2006.

[8] M. Hussein, H. Hunt, *A numerical model for calculating vibration from a railway tunnel embedded in a full-space*, J. Sound Vib., 305, 401-431, 2007.

[9] M. Hussein, H. Hunt, L. Rikse, S. Gupta, G. Degrande, J. Talbot, S. Francois and M. Schevenels, *Using the PiP model for fast calculation of vibration from a railway tunnel in a multi-layered half-space*, Notes on Numerical Fluid Mechanics and Multidisciplinary Design, 99/2008, 136-142, 2008.

[10] X. Sheng, C. Jones and D. Thompson, *Modelling ground-vibration from railways using wavenumber finite- and boundary-element methods*, Proc. R. Soc. A: Mathematical, Physical and Engineering Sciences, 461, 2043-2070, 2005.

[11] K. Kuo, H. Hunt and M. Hussein, *The effect of a twin tunnel on the propagation of ground-borne vibration from an underground railway*, J. Sound Vib., 330, 6203-6222, 2011.

[12] P. Coulier, G. Degrande, G. Lombaert, *The influence of source-receiver interaction on the numerical prediction of traffic induced vibrations*, Proc. of Advances in Environmental Vibration: Fifth International Symposium on Environmental Vibration, Chengdu, China, 20-22 October, 2011.

[13] P. Coulier, G. Degrande, K. Kuo and H. Hunt, *A comparison of two models for the vibration response of piled foundations to inertial and underground-railway-induced loadings*, Proc. of the 17th International Congress on Sound & Vibration, Cairo, Egypt, 18-22 July, 2010.

[14] M. Hussein, H. Hunt, K. Kuo, P. Costa and J. Barbosa, *The use of sub-modelling technique to calculate vibration in buildings from underground railways*, Proc. Inst. IMechE. Part F: J. Rail Rapid Transit, 0(0), 1-12, 2013.

[15] M. Schevenels, S. Francois and G. Degrande, *An ElastoDynamics Toolbox for MATLAB*, Comput. Geosci., 35(80): 1752-1754, 2009.

[16] J. Dominguez, *Boundary Elements in Dynamics*, Computational Mechanics Publications and Elsevier Applied Science, Southampton, 1993.